▌ Endohedral Fullerenes

Sc$_2$O@T_d(19151)-C$_{76}$: Hindered Cluster Motion inside a Tetrahedral Carbon Cage Probed by Crystallographic and Computational Studies

Ting Yang,[a] Yajuan Hao,[b] Laura Abella,[c] Qiangqiang Tang,[a] Xiaohong Li,[a] Yingbo Wan,[a] Antonio Rodríguez-Fortea,*[c] Josep M. Poblet,*[c] Lai Feng,*[b] and Ning Chen*[a]

Abstract: A new cluster fullerene, Sc$_2$O@T_d(19151)-C$_{76}$, has been isolated and characterized by mass spectrometry, UV/Vis/NIR absorption, ^{45}Sc NMR spectroscopy, cyclic voltammetry, and single-crystal X-ray diffraction. The crystallographic analysis unambiguously assigned the cage structure as T_d(19151)-C$_{76}$, which is the first tetrahedral fullerene cage characterized by single-crystal X-ray diffraction. This study also demonstrated that the Sc$_2$O cluster has a much smaller Sc—O—Sc angle than that of Sc$_2$O@C_s(6)-C$_{82}$ and the Sc$_2$O unit is fully ordered inside the T_d(19151)-C$_{76}$ cage. Computational studies further revealed that the cluster motion of the Sc$_2$O is more restrained in the T_d(19151)-C$_{76}$ cage than that in the C_s(6)-C$_{82}$ cage. These results suggest that cage size affects not only the shapes but also the cluster motion inside fullerene cages.

Introduction

Fullerenes are all-carbon compounds consisting of cages with hollow space inside.[1,2] With species encapsulated inside the cage, endohedral fullerenes have been extensively studied since the discovery of La@C$_{82}$ in 1991.[3,4] These compounds have generated considerable recent research interest because of their potential applications in the field of magnetic resonance imaging agents, molecular electronic devices, and solar cells.[5–9] Since the discovery of Sc$_3$N@C$_{80}$ in 1999,[10] cluster fullerenes (CFs) have been of particular interest in the field of endohedral fullerenes as a result of their exceptionally high yield and excellent stability and the unique structural variety of both clusters and cages, which results in their tunable physical and chemical properties.[11–14] To date, a variety of cluster fullerenes have been reported, including nitride (NCFs),[15–17] carbide (CCFs),[18,19] hydrocarbide (HCCFs),[20] oxide (OCFs),[21,22] sulfide (SCFs),[23–25] carbonnitride (CNCFs),[26,27] and di/trimetallic cluster fullerenes.[28,29] In particular, the OCF family has demonstrated exceptional structural versatility of the encapsulated oxide clusters, which have included Sc$_2$O,[21] Sc$_4$O$_2$,[22] and Sc$_4$O$_3$[30] structures. In contrast, the reported cage structures of this family have been limited to I_h(7)-C$_{80}$, C_s(6)-C$_{82}$, and the very recent C_2(7892)-C$_{70}$ cages.[31] Other cage structures still remain unexplored.

Very recently, by following the strategy of 'reactive gas atmosphere',[14,25] we prepared an extensive OCF family (that is, Sc$_2$O@C$_{2n}$, $n = 35$–47) by using CO$_2$ as the oxygen source, which renders us with opportunities to explore OCFs with cages beyond I_h(7)-C$_{80}$ and C_s(6)-C$_{82}$.[31] Fullerene cages with high symmetry (that is, I_h) are of great importance because of their possible superconductivity and ferromagnetism.[9] Among them, the T_d-C$_{76}$ carbon cage, which features the third highest symmetry after I_h and I symmetry, has attracted great interest.[32] Nevertheless, though several theoretical and spectroscopic studies have been devoted to the characterization of T_d-C$_{76}$, besides a functionalized C_s-(T_d-C$_{76}$(CF$_3$)$_{12}$),[33] Lu$_2$@T_d-C$_{76}$ is the only discovered species so far.[32,34–36] Moreover, the studies of Lu$_2$@T_d-C$_{76}$ did not provide a detailed structural analysis because of the lack of unambiguous single-crystal X-ray characterization. Thus, further study is very necessary to reveal the structural features of the T_d-fullerenes.

Herein, we report a new member of the OCF family, Sc$_2$O@C$_{76}$. A combined study of UV/Vis/NIR absorption, single-crystal X-ray characterization, and theoretical calculations unambiguously assigned the cage structure as Sc$_2$O@T_d(19151)-C$_{76}$. This work offers not only the first crystallographic observa-

[a] T. Yang,+ Q. Tang, Prof. Dr. X. Li, Y. Wan, Prof. Dr. N. Chen
Laboratory of Advanced Optoelectronic Materials
College of Chemistry, Chemical Engineering and Materials Science
Soochow University, Suzhou, Jiangsu, 212163 (China)
E-mail: chenning@suda.edu.cn

[b] Y. Hao,+ Prof. Dr. L. Feng
College of Physics, Optoelectronics and Energy and
Collaborative Innovation Center of Suzhou Nano Science and Technology
Soochow University, Suzhou 215006 (China)
E-mail: fenglai@suda.edu.cn

[c] L. Abella,+ Dr. A. Rodríguez-Fortea, Prof. Dr. J. M. Poblet
Departament de Química Física i Inorgànica, Universitat Rovira i Virgili
c/Marcel·lí Domingo 1, 43007 Tarragona (Spain)
E-mail: josepmaria.poblet@urv.cat
antonio.rodriguezf@urv.cat

[+] These authors contributed equally to this work.

🖥 Supporting information for this article is available on the WWW under http://dx.doi.org/10.1002/chem.201500904.

tion of a tetrahedral-symmetry fullerene cage but also a better understanding of the interaction between the endohedral dimetallic oxide cluster and the isolated pentagon rule (IPR) carbon cage. In addition, the current study revealed a hindered cluster motion for $Sc_2O@T_d(19151)$-C_{76}, probably as a result of the compression effect of the small $T_d(19151)$-C_{76} cage.

Results and Discussion

Preparation and purification

The OCFs were synthesized in a conventional Krätschmer–Huffman reactor with an atmosphere of helium and CO_2. The as-produced soot was Soxhlet extracted with chlorobenzene and the raw extract was subjected to multistage HPLC to purify the $Sc_2O@C_{76}$ (Figure S2 in the Supporting Information). $Sc_2O@C_{76}$ was obtained as the third most abundant fullerene in the OCF family after $Sc_2O@C_{82}$ and $Sc_2O@C_{78}$ and the product yield of this compound is around one-third of that obtained for $Sc_2O@C_{82}$.

The MALDI-TOF spectrum of the isolated fraction shows a single peak at m/z 1018.028 (Figure 1). This molecular weight and the isotopic distribution of the experimental MALDI-TOF spectrum show excellent agreement with the corresponding theoretical prediction.
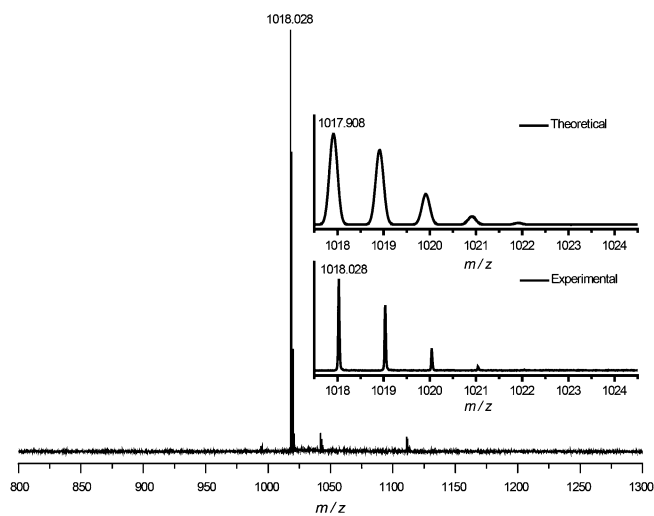

Figure 1. Mass spectra of the purified $Sc_2O@C_{76}$. Inset: experimental and theoretical isotopic distributions for $Sc_2O@C_{76}$.

Structure of $Sc_2O@T_d(19151)$-C_{76} as determined by single-crystal X-ray diffraction

A cocrystal of $Sc_2O@C_{76}$/[Ni^{II}(OEP)] (OEP: octaethylporphyrin) suitable for X-ray analysis was successfully obtained by slow diffusion of a benzene solution of $Sc_2O@C_{76}$ into a $CHCl_3$ solution of [Ni^{II}(OEP)]. The molecular structure was resolved and refined in the monoclinic space group $C2/m$ (No. 12). Figure 2 shows the structure of the endohedral fullerene and its relationship to the nickel porphyrin. In this case, the crystallographic data clearly indicate the presence of the $T_d(19151)$-C_{76}

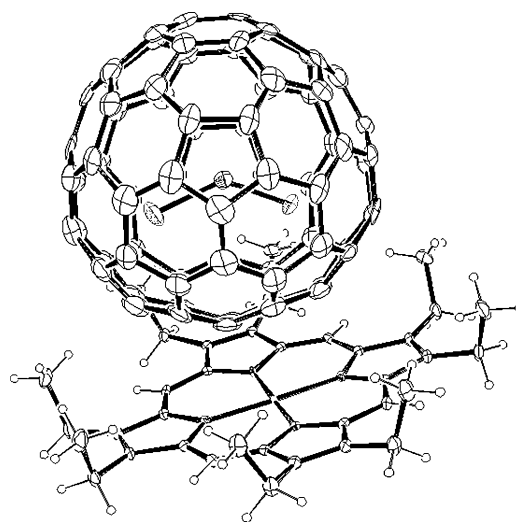**Figure 2.** Ortep drawing of $Sc_2O@T_d(19151)$-C_{76}/[Ni^{II}(OEP)] with 25% thermal ellipsoids, which shows the relationship between the fullerene cage and [Ni^{II}(OEP)]. Only the major cage orientation with 0.371 occupancy and the major Sc_2O unit with the same occupancy are shown. For clarity, the solvent molecules, minor cage orientation, and minor Sc_2O unit are omitted.

cage in this endohedral structure despite the fact that the cage is disordered. To the best of our knowledge, this is the first report of the crystallographic observation of the T_d-C_{76} cage and a tetrahedral-symmetry fullerene.

Two cage orientations were identified with a ratio of 0.371:0.129. Generally, the adjacent [Ni^{II}(OEP)] moiety is approaching the flat region of the fullerene cage. In this case, the distances between the nickel ion in [Ni^{II}(OEP)] and the closest carbon ion in the major and minor cage orientations are 2.790 and 2.793 Å, respectively; these values are similar to those found in most EMF/[Ni^{II}(OEP)] (EMF: endohedral metallofullerene) cocrystals, which suggests similar interactions between EMFs and [Ni^{II}(OEP)].

Inside the fullerene cage, two Sc_2O units were identified. Nevertheless, the initial refinements suggested that the ratio of these two Sc_2O units was similar to that in disordered cages. Thus, it was facile to assign each Sc_2O unit to the cage with similar occupancy and the two together were treated as a set in the final refinement. In other words, the Sc_2O unit is fully ordered relative to each cage orientation. This is different from what was obtained from the crystallographic studies of $Sc_2O@C_s(6)$-C_{82}, in which relative orientations between the cluster and cage are disordered. This difference suggests that the internal motion of Sc_2O might be more restrained in a smaller C_{76} cage than that in the C_{82} cage.

Within the major Sc_2O unit (0.371 occupancy), the Sc–O distances are 1.972(4) Å for Sc1 and 1.825(5) Å for Sc2; the Sc1–O1–Sc2 angle is 133.9(4)°. For the minor Sc_2O unit (0.129 occupancy), slightly longer Sc–O distances (that is, 2.005(10) Å for Sc3 and 1.912(15) Å for Sc4) and a comparable Sc3–O1–Sc4 angle (129.9(6)°) are observed. Further comparison between this $Sc_2O@T_d(19151)$-C_{76} and the previously reported $Sc_2O@C_s(6)$-C_{82} reveals that their endohedral Sc–O distances are almost equal, whereas the Sc–O–Sc angle in $T_d(19151)$-C_{76}

is much smaller than that in $C_s(6)$-C_{82} (156.6(3)°), probably because of the compressing effect of the smaller fullerene cage. These results suggest that cage size plays an important role in the shape of the endohedral Sc_2O cluster.

However, as a result of the crystallographic mirror plane being mismatched with the molecular symmetry, the relative orientation between the Sc_2O cluster and cage cannot be determined from the crystallographic data alone. In fact, inside the major cage, either the major cluster shown in Figure 2 or that generated through the crystallographic mirror plane is equally suggested by X-ray analysis. Theoretical calculations were employed to determine the absolute structure of $Sc_2O@T_d$-C_{76}.

Computational studies

Besides the crystallographic characterization, we have performed a computational study, which confirms that $Sc_2O@T_d(19151)$-C_{76} is the most abundant OCF, among the 19151 possible isomers of C_{76}, for the whole range of temperatures. First of all, the structure for $Sc_2O@T_d(19151)$-C_{76} was optimized at the DFT BP86/TZP level by using the Amsterdam Density Functional (ADF) code (see the Supporting Information for more details).[37–40] Structural parameters very similar to those found for the X-ray structure were obtained; for example, values of 1.884 Å for the Sc—O distance and 146.9° for the Sc—O—Sc angle can be compared to the values found from X-ray crystallography of 1.825–1.972 Å and 133.9°, respectively (Figure 3).
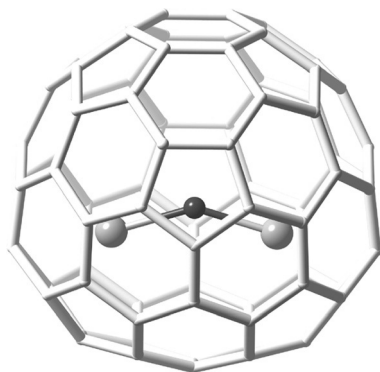

Figure 3. DFT-optimized structure of $Sc_2O@T_d(19151)$-C_{76}.

From an analysis of the frontier molecular orbitals of $Sc_2O@T_d(19151)$-C_{76}, we have verified that a formal transfer of four electrons from Sc_2O to the C_{76} cage takes place, $(Sc_2O)^{4+}$ $@(C_{76})^{4-}$, as shown in the orbital interaction diagram in Figure 4. The HOMO and LUMO are mainly localized on the C_{76} framework, so the first oxidation and reduction take place in the cage (see below). Therefore, the electronic structure can be explained by the ionic model with a formal transfer of four electrons from the cluster to the cage, as for the rest of the cluster fullerenes containing Sc_2X (X: O or S) that are known so far.[21, 24, 25, 41]
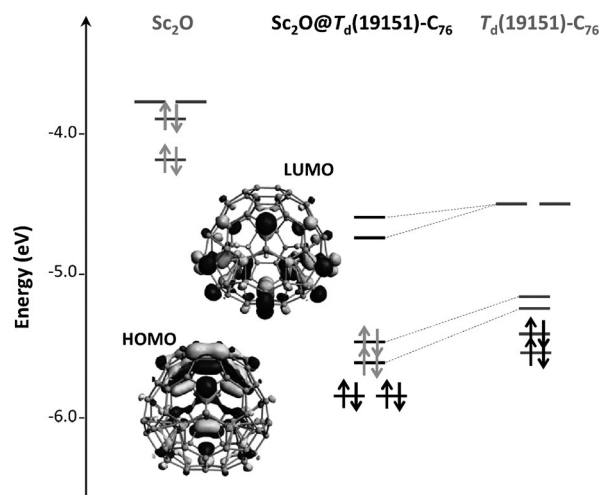

Figure 4. Orbital interaction diagram for $Sc_2O@T_d(19151)$-C_{76}. The fragments Sc_2O and $T_d(19151)$-C_{76} are calculated with the geometry that they have in the OCF.

We have also computed (BP86/TZP) the energies of the tetra-anions for all cages with two or fewer adjacent pentagon pairs (APPs): 2 IPR isomers, 12 APP1 isomers, and 134 APP2 isomers. The lowest-energy tetra-anionic cages, within a range of 40 kcal mol^{-1}, were selected and the corresponding $Sc_2O@C_{76}$ structures were optimized. Different orientations of the Sc_2O cluster in IPR and APP1 cages were taken into account. The IPR cage $T_d(19151)$-C_{76} was found to be, by a large difference, the lowest-energy tetra-anion and the lowest-energy OCF as well (Table 1). The non-IPR $C_{76}(19138)$, with a single APP, is the second most stable isomer for both tetra-anions and OCFs (at 13.7 kcal mol^{-1}). These cages show the lowest number of pyracylenes within the IPR and APP1 subsets, as is usually found for the most stable and characterized cluster fullerenes.[42, 43] As a general trend for the lowest-energy isomers shown in Table 1, the relative stabilities of the OCFs (fourth column) are somewhat smaller than those of the tetraanions (third column), which might indicate that the interactions between Sc_2O and non-IPR cages are more favorable than those with IPR cages. This stabilization, however, is not enough to reverse the stability trend predicted by the ionic model, that is, for tetra-anions, as found for other cluster fullerenes.[41]

The molar fractions of the lowest-energy $Sc_2O@C_{76}$ isomers as a function of the temperature were also computed by using the rigid rotor and harmonic oscillator (RRHO) approximation and the related free-encapsulating model (FEM) as proposed by Slanina et al.[44, 45] The two approximations predict $Sc_2O@T_d(19151)$-C_{76} as the most abundant isomer for the whole temperature range up to 4000 K, in good agreement with the X-ray crystallography results (Figure 5 and the Supporting Information). The abundance of isomer $Sc_2O@C_{2v}(19138)$-C_{76} increases slightly at very high temperatures but only to around 15% of the total. This result is in striking contrast with the predictions made by Zhao, Nagase, and co-workers for the detected but not-yet-characterized $Sc_2S@C_{76}$, in which $Sc_2S@T_d(19151)$-C_{76} was the lowest-energy

Table 1. Relative energies for the lowest-energy isomers of C_{76}^{4-} and $Sc_2O@C_{76}$.[a]

Isomer	APP	Relative energies [kcal mol^{-1}]	
		C_{76}^{4-}	$Sc_2O@C_{76}$
19151	0	0.0	0.0
19138	1	15.5	13.7
17459	1	24.5	20.2
17750	1	31.8	22.7
17894	1	31.6	25.4
17418	1	30.9	25.6
17491	2	30.1	26.8
19142	1	29.5	28.3
17508	2	32.1	28.6
17490	2	19.8	29.8
17465	2	28.1	30.7
19150	0	32.9	31.0

[a] Isomer number according to the spiral algorithm of Fowler and Monopoulos. APP: number of adjacent pentagon pairs.
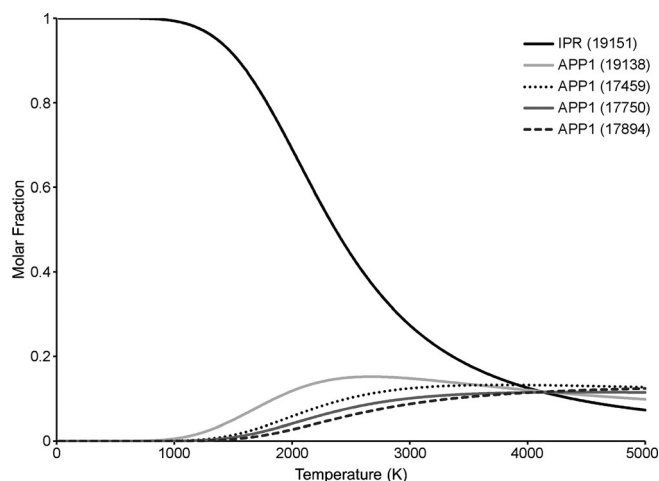
Figure 5. Predicted molar fractions within the FEM approximation as a function of temperature for the five most abundant isomers of $Sc_2O@C_{76}$ (see the Supporting Information for more details).

isomer at 0 K but an inversion of the relative abundances was observed at high temperatures.[34]

Car–Parrinello molecular dynamics simulations (see the Supporting Information for more details) at the temperature of crystallographic determination (80 K), room temperature, and the temperature of fullerene formation (2000 K) were also done to gain more insight about the motion of the Sc_2O cluster inside the fullerene.[46] For trajectories that last 14 ps, we have seen that the Sc_2O unit is moving inside the cage, with smaller or larger amplitudes that depend on the simulation temperature (Figure 6). At 2000 K, the mobility of the Sc_2O unit to equivalent positions in the highly symmetric fullerene cage is much more evident, as shown in Figure 6. The average Sc—O—Sc angle for the trajectory at 80 K reasonably coincides with the value found by X-ray crystallography (molecular dynamics: 130.0°; experimental: 133.9°), with oscillations of around 10°. Such oscillations become much more marked at higher tem-

peratures (100–180° at 2000 K), which confirms the high flexibility of the Sc_2O unit inside this cage. To help in the determination of the absolute structure of $Sc_2O@T_d(19151)$-C_{76}, the two equally suggested orientations of Sc_2O by X-ray analysis were used as starting geometries for two additional Car–Parrinello simulations at 80 K. In one trajectory, the Sc_2O cluster essentially keeps the original (optimal) orientation during 7.2 ps. For the other, however, the cluster changes the initial orientation to get finally the optimal one in 1.5 ps, which shows that there is only one minimum-energy orientation for the isolated molecule. These results are in agreement with the geometry optimizations at the BP86/TZP level (see the Supporting Information).
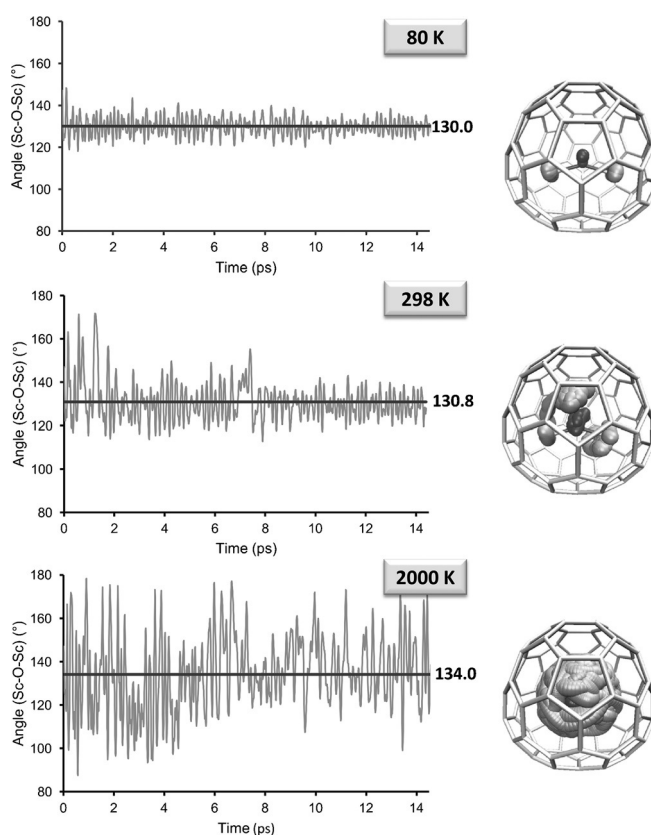

Figure 6. Representation of the motion of the Sc_2O cluster inside the T_d-C_{76} cage during 14 ps-long Car–Parrinello molecular dynamics trajectories at 80, 298, and 2000 K (right), as well as the variation of the Sc—O—Sc angle along the trajectories (left).

Spectroscopic characterization: UV/Vis/NIR and ^{45}Sc NMR spectroscopy

The purified sample has a deep-green color in toluene and CS_2 solution. The sample dissolved in the CS_2 solution was further characterized by UV/Vis/NIR absorption (Figure 7). The characteristic features of this spectrum include major absorption peaks at 651, 713, and 836 nm, along with two broad absorptions at 1136 and 1377 nm. These features are very similar to those reported for $Lu_2@C_{76}$, which suggests an identical cage structure shared by the two endohedral fullerenes.[32] On the

other hand, these absorption features are essentially different from those of $DySc_2N@C_s(17490)$-C_{76}, which indicates a major difference in the cage symmetry and the charge transfer between the clusters and outside carbon cages.[47] On the basis of absorption onset at 1587 nm, the optical bandgap of this compound was estimated to be 0.79 eV. By using 1.0 eV as the limit to distinguish large- and small-bandgap fullerenes, we can assign this isomer of $Sc_2O@T_d(19151)$-C_{76} as a small-bandgap fullerene. This bandgap is notably smaller than that of $DySc_2N@C_s(17490)$-C_{76} (0.96 eV), which again suggests a major difference in the electronic structures of the two C_{76}-based cluster fullerenes. On the other hand, although the two fullerenes share the same cage symmetry, the bandgap for $Sc_2O@T_d(19151)$-C_{76} is larger than that of 0.69 eV for $Lu_2@T_d$-C_{76}, which verifies again the significant impact of the encaged species on the electronic structures of endohedral fullerenes. The HOMO–LUMO gaps for these two endohedral fullerenes that share the same high-symmetry C_{76} cage correlate with the experimental optical bandgaps: 0.75 eV for $Sc_2O@T_d(19151)$-C_{76} and 0.45 eV for $Lu_2@T_d$-C_{76}. The computed UV/Vis/NIR spectrum from time-dependent DFT calculations in the Vis/NIR region (wavelengths larger than 500 nm) shows reasonable agreement with the experimental one (Figure S7 in the Supporting Information), despite the limitations of the methodology, as found for the SCF family.[24,41] There are no UV/Vis/NIR data reported for other OCFs to be compared with, but the bandgap of $Sc_2O@T_d(19151)$-C_{76} is smaller than all those of SCFs reported so far, including $Sc_2S@C_s(10528)$-C_{72} and two isomers of $Sc_2S@C_{82}$, in line with the computed HOMO–LUMO gaps.[24,25,41]

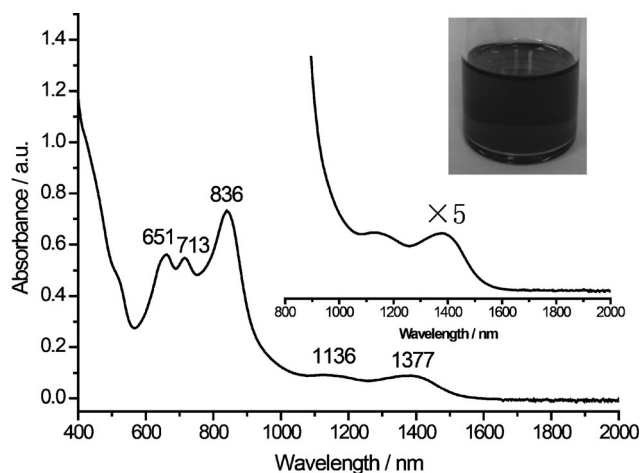**Figure 7.** UV/Vis/NIR absorption spectrum of $Sc_2O@T_d(19151)$-C_{76} in CS_2 solution. The insets show an enlarged spectral range (1000–1600 nm) and the photograph of $Sc_2O@T_d(19151)$-C_{76} dissolved in CS_2.

We also carried out the first ^{45}Sc NMR spectroscopy studies on the OCF family. As Figure 8 shows, a single line at $\delta = 76.9$ ppm was recorded in the ^{45}Sc NMR spectrum of $Sc_2O@C_{76}$. The single signal for ^{45}Sc suggests that the two Sc atoms in the Sc_2O cluster are essentially equivalent, which agrees with the significant rotation of the cluster at room temperature (see above) and the proposed highly symmetrical outside cage. On

the other hand, compared with the values obtained for SCFs, the chemical shift of ^{45}Sc for $Sc_2O@T_d(19151)$-C_{76} is significantly different from $\delta = 290$ ppm for $Sc_2S@C_{3v}(8)$-C_{82} and $\delta = 183.3$ ppm for $Sc_2S@C_s(10528)$-C_{72}.[23,24] It is evident that the different cages will have a major impact on the ^{45}Sc chemical shift, as observed for SCFs. However, the bond difference between the Sc_2O cluster and Sc_2S cluster is also likely to contribute to this major chemical shift difference between that of $Sc_2O@T_d(19151)$-C_{76} and those of the above-mentioned SCFs. The computed ^{45}Sc NMR signals for $Sc_2O@T_d(19151)$-C_{76} and $Sc_2S@C_s(10528)$-C_{72} ($\delta = -132$ and -28 ppm with respect to $Sc_3N@I_h(7)$-C_{80}), although somewhat shifted from the experimental ones ($\delta = -120$ and -14 ppm), reproduce very well their difference (theoretical: $\Delta\delta = 103$ ppm; experimental: $\Delta\delta = 106$ ppm).
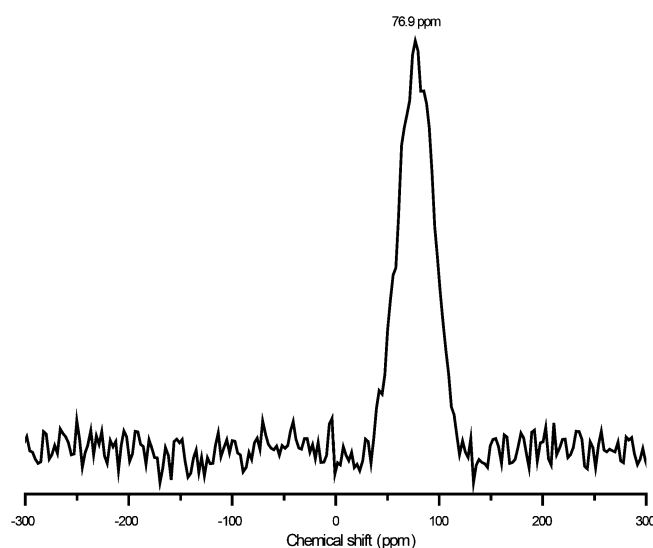

Figure 8. ^{45}Sc NMR spectrum of $Sc_2O@T_d(19151)$-C_{76}.

Electrochemical studies

The cyclic voltammogram of $Sc_2O@T_d(19151)$-C_{76} exhibits five reduction peaks and one oxidation peak (Figure 9). The first reduction process and oxidation process are electrochemically reversible, which agrees with the theoretical results predicting that both the first reduction and the oxidation processes are cage based instead of cluster based (see above). For the oxidation processes, a second minor re-reduction peak, which does not exist in the first oxidation process, appeared as the oxidation processes swept further to 0.75 V. This might suggest that a hidden second oxidation process, which is not evident in the CV scan range, is electrochemically irreversible. In the reduction processes, the second and third reduction peaks are essentially overlapping with each other and are obviously irreversible. The fourth reduction process, however, turned out to be electrochemically reversible again, which is a rare case in the study of the electrochemical behavior of the cluster fullerenes.[9,48]

Up to now, electrochemical studies of OCFs have been carried out for only two structures, $Sc_4O_2@I_h(7)$-C_{80} and

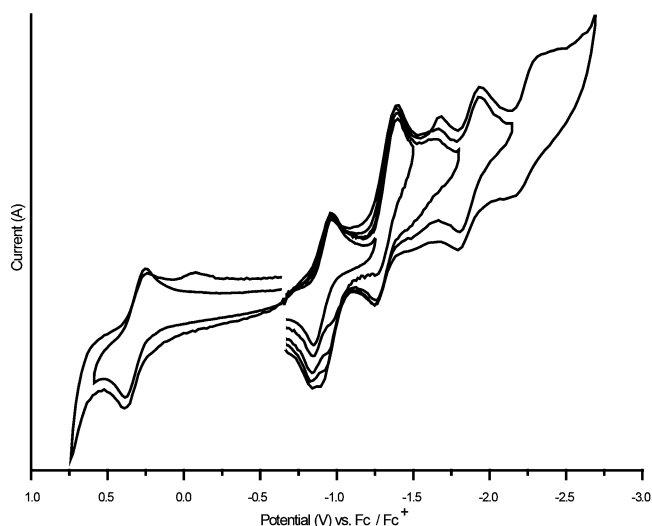**Figure 9.** Cyclic voltammograms of $Sc_2O@T_d(19151)$-C_{76} in (nBu)$_4$NPF$_6$/1,2-dichlorobenzene (o-DCB) with ferrocene as the internal standard; scan rate: 100 mV s^{-1}.

Effect of the cage on the oxide cluster: $Sc_2O@T_d(19151)$-C_{76} versus $Sc_2O@C_s(6)$-C_{82}

$Sc_2O@T_d(19151)$-C_{76} is the second crystallographic observation of dimetallic oxide cluster fullerenes after $Sc_2O@C_s(6)$-C_{82}, which offers a unique opportunity for us to experimentally compare the two endohedral structures in detail and unveil the cage–cluster interactions. The comparative studies of the Sc—O—Sc angles of $Sc_2O@T_d(19151)$-C_{76} and $Sc_2O@C_s(6)$-C_{82} have demonstrated that, with a smaller cage, the Sc—O—Sc angle is considerably decreased as a result of the compressing effect of the smaller fullerene cage. This result is consistent with recent computational studies for Sc$_2$S by Deng and Popov, in which the carbon cage for Sc$_2$S@C$_{2n}$ structures was found to be able to dictate the shape adopted by Sc$_2$S without a pronounced increase in energy.[51] A similar effect has also been reported by Dorn and co-workers in the studies of cage–cluster interactions in Y$_2$C$_2$@C$_{2n}$, in which a 'nanoscale fullerene compression' was observed by combined theoretical and NMR studies.[52] Besides cluster conformation, the carbon cage struc-

$Sc_2O@C_s(6)$-C_{82}.[8,49] $Sc_4O_2@I_h(7)$-C_{80} demonstrated cluster-based electrochemical processes, which agrees with the localization of the HOMO and LUMO orbitals on the oxide cluster.[8,50] $Sc_2O@C_s(6)$-C_{82}, on the other hand, shows cage-based redox processes.[49] The electrochemical behavior of $Sc_2O@T_d(19151)$-C_{76} shows much more similarity to that of $Sc_2O@C_s(6)$-C_{82} rather than $Sc_4O_2@I_h(7)$-C_{80}. The computed HOMO and LUMO orbitals (Figure 5), as well as the spin density on the reduced and oxidized states of $Sc_2O@T_d(19151)$-C_{76}, confirm that the first reduction and oxidation of $Sc_2O@T_d(19151)$-C_{76} are also cage-based processes (see the Supporting Information). The computed first cathodic and first anodic potentials (-1.00 and 0.15 V), the second cathodic potential (-1.49 V), and the electrochemical gap (1.15 V) agree reasonably well with the experimental results, within the typical error found for other families of cluster fullerenes.[41,50] However, the structural differences between the $T_d(19151)$-C_{76} and $C_s(6)$-C_{82} cages seemingly did not bring about major differences in their first reduction and oxidation processes. As shown in Figure 9 and Table 2, both the redox pattern and the redox potentials of the first redox processes of these two structures are very similar to each other. The differences between the rest of the reduction processes of $Sc_2O@C_{76}$ and $Sc_2O@C_{82}$ are much more evident, because the overall reduction pattern shows major differences between the cyclic voltammograms of the two structures. In particular, whereas $Sc_2O@C_{82}$ shows well-defined quasireversible second and third reduction processes, the second and third reduction processes of $Sc_2O@C_{76}$ are obviously irreversible.

Table 2. Redox potentials of $Sc_2O@T_d(19151)$-C_{76}, $Sc_2O@C_s(6)$-C_{82}, $Sc_2S@C_s(6)$-C_{82}, and $Sc_2S@C_{3v}(8)$-C_{82} in (nBu)$_4$NPF$_6$/o-DCB with ferrocene as the internal standard.

Compound	$E^{0/+}$ [V]	$E^{0/-}$ [V]	$E^{-/2-}$ [V]	$E^{2-/3-}$ [V]	$E^{3-/4-}$ [V]	$E^{4-/5-}$ [V]	$\Delta E_{gap,ec}$ [V]
$Sc_2O@T_d(19151)$-C_{76}	$+0.32$[a]	-0.91[a]	-1.40[b]	-1.65[b]	-1.93[b]	-2.30[b]	1.23
$Sc_2O@C_s(6)$-C_{82}	$+0.35$[a]	-0.96[a]	-1.28[a]	-1.74[b]			1.31
$Sc_2S@C_s(6)$-C_{82}	$+0.39$[a]	-0.98[a]	-1.12[a]	-1.73[b]			1.37
$Sc_2S@C_{3v}(8)$-C_{82}	$+0.52$[a]	-1.04[b]	-1.19[b]	-1.63[b]			1.56

[a] Half-wave potential (reversible redox process). [b] Peak potential (irreversible redox process).

ture has also been found to have a major effect on the motion of the clusters inside the cage. It is commonly observed inside non-IPR cages, in which the endohedral cluster motion is largely restrained as a result of the strong metal–pentalene interaction, which does not exist in IPR cages. However, to the best of our knowledge, the influence of cage size on the motion of the cluster inside an IPR cage has rarely been addressed before. An exceptional feature of $Sc_2O@T_d(19151)$-C_{76} is that the cluster is completely ordered relative to the carbon cage. In the case of $Sc_2O@C_s(6)$-C_{82}, however, the crystallographic studies showed that the cluster is disordered inside the cage. This difference suggested that, even without the strong metal–pentalene interaction, in the IPR cages, a smaller cage size can somehow restrain the rotation of the Sc_2O cluster. Car–Parrinello molecular dynamics simulations at 80 K for $Sc_2O@T_d(19151)$-C_{76} and $Sc_2O@C_s(6)$-C_{82} confirm the more-hindered motion of Sc_2O inside the smaller $T_d(19151)$-C_{76} cage, which is observed even at the short timescale simulated here (60 ps; see the Supporting Information). Oscillations of the Sc—O—Sc angle along the trajectory, as well as the movement of the whole cluster in the interior of the cage, measured by the root mean square deviation of the Sc and O atoms (see the Supporting Informa-

tion), are significantly larger for $Sc_2O@C_s(6)$-C_{82} than those for $Sc_2O@T_d(19151)$-C_{76}. Thus, these results suggest that the fullerene cage compression not only influences the shape of the cluster but also hinders the cluster motion inside IPR cages.

Conclusions

A new metallic oxide cluster fullerene, $Sc_2O@T_d(19151)$-C_{76}, has been isolated and characterized by mass spectrometry, UV/Vis/NIR absorption spectroscopy, cyclic voltammetry, ^{45}Sc NMR spectroscopy, DFT calculations, and single-crystal X-ray diffraction. For the first time, the single-crystal X-ray diffraction clearly demonstrated the detailed structure of an ordered Sc_2O cluster inside a highly symmetric T_d-C_{76} cage. The Sc−O−Sc angle in $T_d(19151)$-C_{76} was found to be much smaller than that in $C_s(6)$-C_{82}, probably as a result of the compressing effect of the smaller fullerene cage. Computational studies show that the Sc_2O cluster transfers four electrons to the C_{76} cage, $(Sc_2O)^{4+}@C_{76}^{4-}$. $T_d(19151)$-C_{76} is the most stable cage for both empty C_{76}^{4-} and $Sc_2O@C_{76}$, which remains as the most abundant isomer in the whole range of temperatures. We find again here, for the C_{76} family, that the selection of a given cage isomer by a cluster is mainly driven by the formal charge transfer, provided that size effects, that is, large clusters, do not invert the stability trend given by the ionic model. The IPR $T_d(19151)$-C_{76} cage is the selected isomer for those clusters that formally transfer four electrons, as proposed previously for the characterized $Lu_2@C_{76}$,[35] whereas the non-IPR $C_s(17490)$-C_{76} cage, with two APPs, is the cage selected by clusters that transfer six electrons (M_3N, La_2). Moreover, the comparative studies of $Sc_2O@T_d(19151)$-C_{76} and $Sc_2O@C_s(6)$-C_{82}, supported by both crystallographic and computational observations, suggest that the motion of the Sc_2O is more restrained inside the smaller $T_d(19151)$-C_{76} cage than in the $C_s(6)$-C_{82} cage. This observation indicates that the cage size affects not only the shapes but also the cluster motion inside the carbon cages.

Experimental Section

General instruments

The separation and purification of $Sc_2O@T_d(19151)$-C_{76} were performed by multistep HPLC by using an LC-9230 II NEXT machine (Japan Analytical Industry Co., Ltd.) with toluene as the mobile phase. MALDI-TOF mass spectrometry was performed by using an Ultraflextreme spectrometer (Bruker Daltonics, Germany). UV/Vis/NIR spectra were measured in CS_2 by using a UV-3600 spectrophotometer (Shimadzu Corp., Japan). Cyclic voltammetry was performed in o-DCB with 0.5 M $(nBu)_4NPF_6$ at a Pt working electrode with a Zahner Zennium workstation (Zahner, Germany). The ^{45}Sc NMR spectroscopic measurements were performed at 145 MHz with an Agilent Direct-Drive II 600 MHz spectrometer (Agilent, USA) at room temperature in CS_2 with D_2O as the lock and a 0.4 M $Sc(NO_3)_3$ solution in D_2O as the reference.

Preparation and isolation of $Sc_2O@T_d(19151)$-C_{76}

The OCFs were synthesized in a conventional DC arc-discharge Krätschmer–Huffman reactor. A graphite anode doped with Sc_2O_3

and graphite powder (23:40 wt/wt ratio) was burned, along with a graphite rod as the countered cathode, in the arcing chamber under a 200 Torr He and 20 Torr CO_2 atmosphere. The as-produced soot was extracted with chlorobenzene. A multistage HPLC procedure was utilized to isolate and purify $Sc_2O@C_{76}$. A Buckyprep-M column (10×250 mm, Cosmosil, Nacalai Tesque Inc.) was employed for the first-stage separation and a Buckyprep column (10×250 mm, Cosmosil, Nacalai Tesque Inc.) was employed for the second-stage separation. The final separation and purification of $Sc_2O@C_{76}$ was accomplished by a third step with a Buckyprep-M column (10×250 mm, Cosmosil, Nacalai Tesque Inc.).

Single-crystal X-ray structure analysis

Black crystals of $Sc_2O@$ $C_{76}/[Ni^{II}(OEP)]$ were obtained by layering a saturated solution of the EMF in benzene over a solution of $[Ni^{II}(OEP)]$ in trichloromethane in a glass tube at 273 K for 15 d. The crystal was mounted on Cryoloops with paratone and optically aligned on a Bruker D8-Venture single-crystal X-ray diffractometer equipped with a Turbo X-ray Source ($Mo_{K\alpha}$ radiation, $\lambda = 0.71073$ Å) with the direct-drive rotating anode technique and a complementary metal–oxide–semiconductor detector under 123 K.

Crystal data for $Sc_2O@T_d(19151)$-$C_{76}\cdot Ni^{II}(OEP)\cdot 0.88\,C_6H_6\cdot 0.12\,CHCl_3$: $C_{117.40}H_{49.40}Cl_{0.36}Sc_2ON_4Ni$; $Mr = 1693.20$; $0.20\times0.15\times0.10$ mm; monoclinic; $C2/m$ (no. 12); $a = 25.1238(7)$, $b = 14.9617(4)$, $c = 19.5256(6)$ Å; $\beta = 94.1431(9)°$; $V = 7320.4(6)$ Å^3; $Z = 4$; $\rho_{calcd} = 1.551$ g cm^{-3}; $\mu(Mo_{K\alpha}) = 0.520$ mm^{-1}; $\theta = 2.73$–$28.50°$; $T = 123$ K; $R_1 = 0.1218$ and $wR_2 = 0.3118$ for 9492 reflections ($I > 2.0\sigma(I)$) with 1181 parameters; maximum residual electron density: 1.453 e Å^{-3}. CCDC 1047080 ($Sc_2O@T_d$-$C_{76}\cdot[Ni^{II}(OEP)]$) contains the supplementary crystallographic data for this paper. These data are provided free of charge by The Cambridge Crystallographic Data Centre.

Computational details

We have computed all of the tetra-anions of C_{76} with two or less APPs by using DFT methodology with the ADF 2012 program. The exchange-correlation functionals of Becke and Perdew (BP86) and the Slater TZP basis sets were employed. The selected structures of $Sc_2O@C_{76}$ were optimized at the same level of theory. We have computed the UV/Vis/NIR spectrum by using time-dependent DFT in the Vis/NIR region for wavelengths larger than 500 nm. Both were performed at the BP86 level. The ^{45}Sc NMR spectroscopic chemical shifts were calculated at the PBE/TZP level. All of the above calculations were performed with the ADF 2012 program.

Molecular dynamics simulations were carried out by using the Car–Parrinello molecular dynamics program. The description of the electronic structure was based on the expansion of the valence electronic wave functions into a plane wave basis set, which was limited by an energy cutoff of 40 Ry. The interaction between the valence electrons and the ionic cores was treated through the pseudopotential approximation (Martins–Troullier type). The functional by Perdew, Burke, and Ernzerhoff was selected as the density functional. We included the nonlinear core corrections in the Martins–Troullier pseudopotential for the scandium atom. We used a fictitious electron mass of 800 a.u. The simulations were carried out with periodic boundary conditions in a cubic cell with a side length of 15 Å and a time step of 0.144 fs.

Acknowledgements

[1] H. W. Kroto, J. R. Heath, S. C. O'Brien, R. F. Curl, R. E. Smalley, *Nature* **1985**, *318*, 162 – 163.
[2] W. Krätschmer, L. D. Lamb, K. Fostiropoulos, D. R. Huffman, *Nature* **1990**, *347*, 354 – 358.
[3] Y. Chai, T. Guo, C. Jin, R. E. Haufler, L. P. F. Chibante, J. Fure, L. Wang, J. M. Alford, R. E. Smalley, *J. Phys. Chem.* **1991**, *95*, 7564 – 7568.
[4] W. J. Blau, H. J. Byrne, D. J. Cardin, T. J. Dennis, J. P. Hare, H. W. Kroto, R. Taylor, D. R. Walton, *Phys. Rev. Lett.* **1991**, *67*, 1423 – 1425.
[5] J. Dreiser, R. Westerstrom, Y. Zhang, A. A. Popov, L. Dunsch, K. Kramer, S. X. Liu, S. Decurtins, T. Greber, *Chem. Eur. J.* **2014**, *20*, 13536 – 13540.
[6] S. F. Yang, *Curr. Org. Chem.* **2012**, *16*, 1079 – 1094.
[7] X. Lu, L. P. Bao, T. Akasaka, S. Nagase, *Chem. Commun.* **2014**, *50*, 14701 – 14715.
[8] A. A. Popov, N. Chen, J. R. Pinzón, S. Stevenson, L. A. Echegoyen, L. Dunsch, *J. Am. Chem. Soc.* **2012**, *134*, 19607 – 19618.
[9] A. A. Popov, S. Yang, L. Dunsch, *Chem. Rev.* **2013**, *113*, 5989 – 6113.
[10] S. Stevenson, G. Rice, T. Glass, K. Harich, F. Cromer, M. R. Jordan, J. Craft, E. Hadju, R. Bible, M. M. Olmstead, K. Maitra, A. J. Fisher, A. L. Balch, H. C. Dorn, *Nature* **1999**, *401*, 55 – 57.
[11] Y. Zhang, K. B. Ghiassi, Q. M. Deng, N. A. Samoylova, M. M. Olmstead, A. L. Balch, A. A. Popov, *Angew. Chem. Int. Ed.* **2015**, *54*, 495 – 499; *Angew. Chem.* **2015**, *127*, 505 – 509.
[12] D. M. Rivera-Nazario, J. R. Pinzon, S. Stevenson, L. A. Echegoyen, *J. Phys. Org. Chem.* **2013**, *26*, 194 – 205.
[13] A. Rodríguez-Fortea, A. L. Balch, J. M. Poblet, *Chem. Soc. Rev.* **2011**, *40*, 3551 – 3563.
[14] L. Dunsch, S. Yang, *Phys. Chem. Chem. Phys.* **2007**, *9*, 3067 – 3081.
[15] T. Wang, C. Wang, *Acc. Chem. Res.* **2014**, *47*, 450 – 458.
[16] S. Yang, F. Liu, C. Chen, M. Jiao, T. Wei, *Chem. Commun.* **2011**, *47*, 11822 – 11839.
[17] J. Y. Zhang, S. Stevenson, H. C. Dorn, *Acc. Chem. Res.* **2013**, *46*, 1548 – 1557.
[18] C. R. Wang, T. Kai, T. Tomiyama, T. Yoshida, Y. Kobayashi, E. Nishibori, M. Takata, M. Sakata, H. Shinohara, *Angew. Chem. Int. Ed.* **2001**, *40*, 397 – 399; *Angew. Chem.* **2001**, *113*, 411 – 413.
[19] X. Lu, L. Feng, T. Akasaka, S. Nagase, *Chem. Soc. Rev.* **2012**, *41*, 7723 – 7760.
[20] M. Krause, F. Ziegs, A. A. Popov, L. Dunsch, *ChemPhysChem* **2007**, *8*, 537 – 540.
[21] B. Q. Mercado, M. A. Stuart, M. A. Mackey, J. E. Pickens, B. S. Confait, S. Stevenson, M. L. Easterling, R. Valencia, A. Rodríguez-Fortea, J. M. Poblet, M. M. Olmstead, A. L. Balch, *J. Am. Chem. Soc.* **2010**, *132*, 12098 – 12105.
[22] S. Stevenson, M. A. Mackey, M. A. Stuart, J. P. Phillips, M. L. Easterling, C. J. Chancellor, M. M. Olmstead, A. L. Balch, *J. Am. Chem. Soc.* **2008**, *130*, 11844 – 11845.
[23] L. Dunsch, S. Yang, L. Zhang, A. Svitova, S. Oswald, A. A. Popov, *J. Am. Chem. Soc.* **2010**, *132*, 5413 – 5421.
[24] N. Chen, C. M. Beavers, M. Mulet-Gas, A. Rodriguez-Fortea, E. J. Munoz, Y. Y. Li, M. M. Olmstead, A. L. Balch, J. M. Poblet, L. Echegoyen, *J. Am. Chem. Soc.* **2012**, *134*, 7851 – 7860.
[25] N. Chen, M. N. Chaur, C. Moore, J. R. Pinzon, R. Valencia, A. Rodriguez-Fortea, J. M. Poblet, L. Echegoyen, *Chem. Commun.* **2010**, *46*, 4818 – 4820.
[26] T. S. Wang, L. Feng, J. Y. Wu, W. Xu, J. F. Xiang, K. Tan, Y. H. Ma, J. P. Zheng, L. Jiang, X. Lu, C. Y. Shu, C. R. Wang, *J. Am. Chem. Soc.* **2010**, *132*, 16362 – 16364.
[27] S. Yang, C. Chen, F. Liu, Y. Xie, F. Li, M. Jiao, M. Suzuki, T. Wei, S. Wang, Z. Chen, X. Lu, T. Akasaka, *Sci. Rep.* **2013**, *3*, 1487.
[28] W. Xu, L. Feng, M. Calvaresi, J. Liu, Y. Liu, B. Niu, Z. J. Shi, Y. F. Lian, F. Zerbetto, *J. Am. Chem. Soc.* **2013**, *135*, 4187 – 4190.
[29] L. Feng, M. Suzuki, N. Mizorogi, X. Lu, M. Yamada, T. Akasaka, S. Nagase, *Chem. Eur. J.* **2013**, *19*, 988 – 993.
[30] B. Q. Mercado, M. M. Olmstead, C. M. Beavers, M. L. Easterling, S. Stevenson, M. A. Mackey, C. E. Coumbe, J. D. Phillips, J. P. Phillips, J. M. Poblet, A. L. Balch, *Chem. Commun.* **2010**, *46*, 279 – 281.
[31] M. Zhang, Y. Hao, X. Li, L. Feng, T. Yang, Y. Wan, N. Chen, Z. Slanina, F. Uhlík, H. Cong, *J. Phys. Chem. C* **2014**, *118*, 28883 – 28889.
[32] H. Umemoto, K. Ohashi, T. Inoue, N. Fukui, T. Sugai, H. Shinohara, *Chem. Commun.* **2010**, *46*, 5653 – 5655.
[33] N. B. Shustova, I. V. Kuvychko, R. D. Bolskar, K. Seppelt, S. H. Strauss, A. A. Popov, O. V. Boltalina, *J. Am. Chem. Soc.* **2006**, *128*, 15793 – 15798.
[34] P. Zhao, T. Yang, Y. J. Guo, J. S. Dang, X. Zhao, S. Nagase, *J. Comput. Chem.* **2014**, *35*, 1657 – 1663.
[35] T. Yang, X. Zhao, E. Osawa, *Chem. Eur. J.* **2011**, *17*, 10230 – 10234.
[36] R. Ettl, I. Chao, F. Diederich, R. L. Whetten, *Nature* **1991**, *353*, 149 – 153.
[37] E. J. Baerends, D. E. Ellis, P. Ros, ADF **2012**, Department of Theoretical Chemistry, Vrije Universiteit, Amsterdam.
[38] A. D. Becke, *Phys. Rev. A* **1988**, *38*, 3098 – 3100.
[39] A. D. Becke, *J. Chem. Phys.* **1986**, *84*, 4524 – 4529.
[40] G. te Velde, F. M. Bickelhaupt, E. J. Baerends, C. Fonseca Guerra, S. J. A. van Gisbergen, J. G. Snijders, T. Ziegler, *J. Comput. Chem.* **2001**, *22*, 931 – 967.
[41] N. Chen, M. Mulet-Gas, Y. Y. Li, R. E. Stene, C. W. Atherton, A. Rodriguez-Fortea, J. M. Poblet, L. Echegoyen, *Chem. Sci.* **2013**, *4*, 180 – 186.
[42] A. Rodríguez-Fortea, N. Alegret, A. L. Balch, J. M. Poblet, *Nat. Chem.* **2010**, *2*, 955 – 961.
[43] A. Rodríguez-Fortea, J. M. Poblet, *Faraday Discuss.* **2014**, *173*, 201 – 213.
[44] Z. Slanina, S. L. Lee, F. Uhlík, L. Adamowicz, S. Nagase, *Theor. Chem. Acc.* **2007**, *117*, 315 – 322.
[45] Z. Slanina, S. Nagase, *ChemPhysChem* **2005**, *6*, 2060 – 2063.
[46] R. Car, M. Parrinello, *Phys. Rev. Lett.* **1985**, *55*, 2471 – 2474.
[47] S. Yang, A. A. Popov, L. Dunsch, *J. Phys. Chem. B* **2007**, *111*, 13659 – 13663.
[48] M. N. Chaur, F. Melin, A. L. Ortiz, L. Echegoyen, *Angew. Chem. Int. Ed.* **2009**, *48*, 7514 – 7538; *Angew. Chem.* **2009**, *121*, 7650 – 7675.
[49] B. Q. Mercado, N. Chen, A. Rodríguez-Fortea, M. A. Mackey, S. Stevenson, L. Echegoyen, J. M. Poblet, M. M. Olmstead, A. L. Balch, *J. Am. Chem. Soc.* **2011**, *133*, 6752 – 6760.
[50] R. Valencia, A. Rodríguez-Fortea, S. Stevenson, A. L. Balch, J. M. Poblet, *Inorg. Chem.* **2009**, *48*, 5957 – 5961.
[51] Q. Deng, A. A. Popov, *J. Am. Chem. Soc.* **2014**, *136*, 4257 – 4264.
[52] J. Y. Zhang, T. Fuhrer, W. J. Fu, J. C. Ge, D. W. Bearden, J. Dallas, J. Duchamp, K. Walker, H. Champion, H. Azurmendi, K. Harich, H. C. Dorn, *J. Am. Chem. Soc.* **2012**, *134*, 8487 – 8493.